Modeling the Conformer-Dependent Electronic Absorption Spectra and Photolysis Rates of Methyl Vinyl Ketone Oxide and Methacrolein Oxide

Julia C. McCoy¹, Spencer J. Léger¹, Conrad F. Frey¹, Michael F. Vansco², Barbara Marchetti^{1,*}, and Tolga N. V. Karsili^{1,*}

¹Department of Chemistry, University of Louisiana at Lafayette, Louisiana, LA 70503, USA

²Chemical Sciences and Engineering Division, Argonne National Laboratory, Lemont, IL 60439,

USA

*Authors to whom correspondence be addressed:

barbara.marchetti1@louisiana.edu

tolga.karsili@louisiana.edu

Abstract

Criegee intermediates are important atmospheric oxidants, formed via the reaction of ozone with volatile alkenes emitted into the troposphere. Small Criegee Intermediates (e.g. CH₂OO and CH₃CHOO) are highly reactive and removal via unimolecular decay or bimolecular chemistry dominates their atmospheric lifetimes. As the molecular complexity of Criegee Intermediates increases, their electronic absorption spectra show a bathochromic shift within the solar spectrum relevant to the troposphere. In these cases, solar photolysis may become a competitive contributor to their atmospheric removal.

In this manuscript we report the conformer-dependent simulated electronic absorption spectra of two four-carbon centered Criegee Intermediates, methyl vinyl ketone oxide (MVK-oxide) and methacrolein oxide (MACR-oxide). Both MVK-oxide and MACR-oxide contain four low-energy conformers, which are convoluted in the experimentally measured spectra. Here we deconvolute each conformer and estimate contributions from each of the four conformers to the experimentally measured spectra. We also estimate photolysis rates and predict that solar photolysis should be a more competitive removal process for MVK-oxide and MACR-oxide (*cf.* CH₂OO and CH₃CHOO).

Introduction

Criegee intermediates are important atmospheric molecules that have attracted vast attention for at least the last two decades. ^{1–12} Their chemistry is implicated in enhancing the oxidizing capacity of the troposphere as they are well-known sources of non-photolytic OH radicals. ^{6,13–17} They are also implicated in the formulation of highly oxidized compounds and acids which typically condense to form aerosol particles. ^{13,18}

In the atmosphere, Criegee Intermediates are formed via the reaction of volatile alkenes with tropospheric ozone – in a process known as ozonolysis. ^{19–24} Ozonolysis accounts for ca. 10 % of the removal of tropospheric isoprene, which has a total emission of ca. 500 Tg yr⁻¹ – making it the most abundant alkene and second most abundant volatile organic compound emitted into the troposphere. ²⁵ Once formed, the nascent Criegee Intermediate can undergo unimolecular decay or collisional relaxation to form stabilized Criegee Intermediates. The stabilized Criegee Intermediate may then undergo unimolecular decay, bimolecular chemistry ²⁶ or UV-excitation. ^{27–37}

Despite the importance of UV-excitation in atmospheric processes, the UV absorption spectra and photophysics of Criegee Intermediates have received surprisingly little attention in terms of their photolysis rates, molecular dynamics, atmospheric lifetimes, and photochemistries. The electronic absorption spectra of Criegee Intermediates with <C4 have attracted some experimental^{28,30–34,38} and theoretical^{29,35–37} attention. All studies highlight that the absorption spectra of CH₂OO and CH₃CHOO are dominated by a strongly absorbing $\pi\pi*$ state.^{32,33,36,38–42} For such small Criegee Intermediates, UV-excitation may provide a sensitive probe for detection

of these Criegee Intermediates – but is unlikely to be a dominant tropospheric removal process since the UV absorption maxima are outside of the tropospheric actinic flux. ^{28,30–34,38}

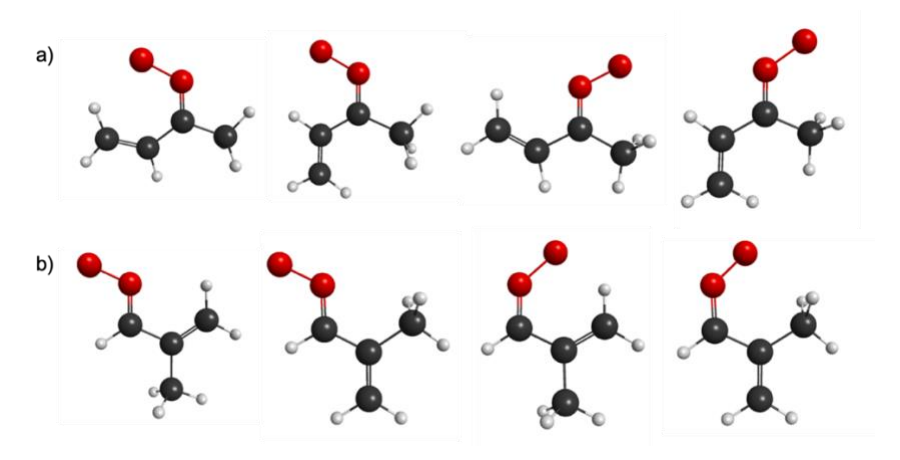


Figure 1: Panel (a) displays methyl vinyl ketone oxide and its four conformers in order left to right AC, AT, SC, ST. Panel (b) similarly displays methacrolein oxide along with its four conformers in order left to right AC, AT, SC, ST.

For larger Criegee Intermediates, UV-excitation may be an important contributor to their tropospheric removal, on a competitive timescale with unimolecular decay and bimolecular chemistry. Methyl vinyl ketone oxide (MVK-oxide) and methacrolein oxide (MACR-oxide) are two such examples of Criegee Intermediates with increased molecular complexity (*cf.* CH₂OO and CH₃CHOO) and are formed via the ozonolysis of isoprene (displayed in Figure 1). As Criegee Intermediates increase in molecular complexity their number of isomeric forms and conformations sharply increase. Previous studies have shown that their reactivities are largely structure dependent. Additionally, each conformer may have a unique UV absorption spectrum and photochemistry. For example, *syn* and *anti-* CH₃CHOO have widely contrasting electronic absorption maxima. The experimental absorption maxima of MVK-oxide and MACR-oxide are bathochromic with respect to those of CH₂OO and CH₃CHOO – overlapping

well within the solar spectrum.^{46,47} Solar photolysis may therefore be a significant contributor to their atmospheric lifetimes.

Computationally, the electronic absorption spectra of CH₂OO and CH₃CHOO has previously been simulated with elegant techniques that range from molecular dynamics simulations to a full quantum mechanical treatment. 35,36,48 These methods are however difficult to extend to larger and more functionalized Criegee Intermediates. In a recently published article, ⁴⁹ we benchmarked the simulated UV absorption spectra of CH₂OO and CH₃CHOO. In that study, we used the nuclear ensemble model to simulate the absorption profiles with a variety of multi- and single- reference electronic structure methods. The nuclear ensemble method has also been used to simulate the electronic absorption spectra of several atmospherically relevant systems. 50-56 The most striking observations from our previous work is the simplicity of computing the electronic absorption profiles and the high-level computations that are modest enough to be feasibly extended to computing analogous UV absorption spectra of larger Criegee Intermediates of increasing molecular complexity. Despite its simplicity, our method of computing the UV absorption profiles of CH₂OO and CH₃CHOO were shown to be qualitatively accurate. In this manuscript we explore the performance of the nuclear ensemble method, coupled with single- and multi-reference electronic structure theory, in simulating the absorption profiles of MVK-oxide and MACR-oxide. In so doing we deconvolute the contribution of the various conformers to the absorption profile in order to estimate the conformer distributions in the experimentally measured electronic absorption spectra. We also estimate the conformerdependent rates for solar photolysis.

Computational Methods

The computation of the electronic absorption spectra of small Criegee Intermediates, using the nuclear ensemble method, was recently reported by us in more detail in ref.⁴⁹ Here, only a brief account will be given. The ground state minimum energy geometry of all four conformers of MVK-oxide and MACR-oxide were optimized using the B3LYP/6-311+G(d,p) level of theory. Based on this optimized geometry, normal mode wavenumbers were computed at the same level. The phase space of the ground state potential energy surface for each conformer was modeled using a 500-point Wigner distribution based on the normal mode eigenvectors of the ground state global minimum using a Newton-X subprogram. 57,58 Vertical excitation energies and transition dipole moments were computed on each geometry returned from the Wigner distribution, using the single state complete active space second-order perturbation theory (CASPT2)^{59–61} method alongside an aug-cc-pVDZ⁶² basis set assigned to all atoms. These were based on a stateaveraged complete active space self-consistent field (SA-CASSCF) reference wavefunction across the lowest seven singlet states. Active spaces of twelve electrons in ten orbitals (12/10), ten electrons in eight orbitals (10/8) and eight electrons in six orbitals (8/6) were benchmarked. An imaginary level shift of $0.3~E_{\rm H}$ was used for all CASPT2 computations in order to mitigate the involvement of intruder states. The active space used for the CASSCF(12/10)/CASPT(12/10) calculations comprised 5 in-plane orbitals (consistiting of two σ , one O(2p), one σ^* and one O(3s) Rydberg orbital) and 5 out-of-plane orbitals (consistiting of three π and two π^*): these are illustrated in figure S4 which displayes the active orbitals for the most stable conformers of MVK-oxide and MACR-oxide.

For comparison, vertical excitation energies and oscillator strengths were also computed using Time-Dependent Density Functional Theory (TDDFT) on each geometry returned from the

Wigner sampling. In these cases, the coulomb-attenuated model Becke-3-parameter-Lee-Yang-Parr (CAM-B3LYP)⁶³ functional, coupled to the 6-311+G(d,p) basis set was used.^{64,65}

The excitation energy dependent photoabsorption cross section P(E) was then obtained using equation 1,

$$P(E) = \frac{\pi e^2}{2m_e c \varepsilon_0} \sum_{j=1}^{M} \left[\frac{1}{N_{TOT}} \sum_{N=1}^{N_{TOT}} f_{ij}^N g(E - \Delta E_{ij}^N, \delta) \right]$$
(1)

where g is a Lorentzian line shape function given by equation 2,

$$g(E - \Delta E_{ij}^{N}, \delta) = \frac{\hbar \delta}{2\pi} \left(\left(E - \Delta E_{ij}^{N} \right)^{2} + \left(\frac{\delta}{2} \right)^{2} \right)^{-1}.$$
 (2)

 f_{ij} is the oscillator strength given by equation 3.

$$f_{ij}^{N} = \frac{2}{3} \left(\Delta E_{ij}^{N} \right) \sum_{\alpha = x, y, z} \left| \mu_{ij}^{N} \right|_{\alpha}^{2} \tag{3}$$

and $\Delta E_{ij}^N = (E_j^N - E_i^N)$, m_e and e are the mass and charge of the electron, respectively, while c is the speed of light. The internal sum in equation 1 is expressed over the set of total Wigner geometries while the external sum includes transitions from the initial state i (the ground state) to final state j (i.e. $S_1, S_2, S_3, \ldots, S_7$ etc.) with respective oscillator strength f_{ij}^N as given by equation 3. δ is a broadening factor, which is arbitrarily set to 0.1 eV for each of the calculated absorption profiles reported herein. In this work, the transition dipole moments (μ) were obtained from the computation of the CASSCF(12/10)/AVDZ wavefunction.

The photochemical loss of MVK-oxide and MACR-oxide upon solar irradiation is estimated using equation (4),

$$k_p = \int_{\lambda_i}^{\lambda_f} \Phi(\lambda) P(E) F(\lambda) d\lambda \tag{4}$$

where k_p is the solar photolysis rate coefficient, $\Phi(\lambda)$ is the photodissociation quantum yield (assumed to be unity), P(E) is the photoabsorption cross section given by equation 1, and $F(\lambda)$ is the solar actinic flux. The k_p is evaluated for each conformer for a range of solar zenith angles $(0^\circ, 20^\circ, 40^\circ, 60^\circ$ and $80^\circ)$ of $F(\lambda)$ obtained from the National Center for Atmospheric Research TUV model. The $F(\lambda)$ at each solar zenith angle considered is fitted by two separate 8-term polynomials (285 to 447.5 nm and 447.5 to 725 nm) to accurately depict its curvature. An example fit to $F(\lambda)$ is provided in the supporting information (Figure S1).

All the CASSCF and CASPT2 computations were performed using the Molpro computation package^{67,68} while all (TD)DFT calculations were undertaken in Gaussian 16.⁶⁹

Results and Discussion

Electronic absorption spectrum of MVK-oxide

Figure 1(a) presents the ground state minimum energy geometries of the four lowest energy conformers of MVK-oxide. As previously reported, all conformers are with their atoms in a common plane. The four conformers arise from rotational isomerization around the carbonyl C-O and alkene C-C bonds and are labelled *syn-trans* (ST), *syn-cis* (SC), *anti-trans* (AT), and *anti-cis* (AC). *Syn* and *anti* are defined by whether the terminal oxygen atom of the carbonyl-oxide moiety is, respectively, orientated towards or away from the methyl group, while *cis* and *trans* are defined as to whether the terminal carbon atom of the alkene moiety is orientated towards or

away from the carbonyl-oxide moiety, respectively. Within these four conformers, the stability is in the order ST > SC > AT > AC.⁷⁰

Figure 2 presents the calculated CASPT2(12/10) electronic absorption profiles of the (a) ST, (b) SC, (c) AT and (d) AC conformers of MVK-oxide, as well as (e) the convoluted spectra of all four conformers, plotted alongside the experimental absorption spectrum measured by Vansco et al. 46 under jet-cooled conditions (green spectral profile) and Caravan et al. 71 under thermal conditions (298 K, blue spectral profile). The spectra of the individual conformers in panels (a) – (d) are normalized so that their peak maxima matches that of the experimentally measured spectra. In contrast, the cumulative spectrum (in panel (e)) is created by first calculating the photoabsorption cross sections of the four individual conformers using equation (1), summing the four resulting spectra (assuming an equal population in all four conformers) and then normalizing the resulting summed spectrum. The oscillator strengths of the individual conformers are therefore maintained in the cumulative spectrum. The sensitivity of the cumulative spectrum to the conformer populations is explored later in this manuscript. Table 1 lists the calculated photoabsorption cross sections at the peak maximum and the photolysis rates of each of the four conformers of MVK-oxide and MACR-oxide. In all conformers of both molecules, the photolysis lifetimes are ca. 2 s, which is shorter than the experimentally derived photolysis rates for CH₂OO and CH₃CHOO.³¹ To the best of our knowledge, no experimental study has accurately reported the photoabsorption cross sections of MVK-oxide and MACR-oxide.

Additional CASPT2 spectral profiles, calculated using the 10/8 and 8/6 active spaces are given in Figure S2 and S3, respectively, of the supporting information. On average CASPT2(12/10) shows the best agreement in both MVK-oxide and MACR-oxide and was computable with a

reasonable expense. We will therefore use the CASPT2(12/10) spectra in the following narrative. CASPT2(12/10) was also found to perform well for simulating the electronic absorption profiles of CH₂OO and CH₃CHOO⁴⁹ and has also been shown to effectively describe the PE profiles along the O-O stretch coordinate of MVK-oxide⁷² and MACR-oxide.⁴⁷ No attempt to simulate the spectra at larger basis sets or active spaces was attempted, however computation of vertical excitation energies (and corresponding oscillator stregths) at the CASPT2(14,11)/AVDZ and CASPT2(16,12)/AVDZ level of theories do not show considerable differences *cf*. CASPT2(12/10)/AVDZ (v. table S8).

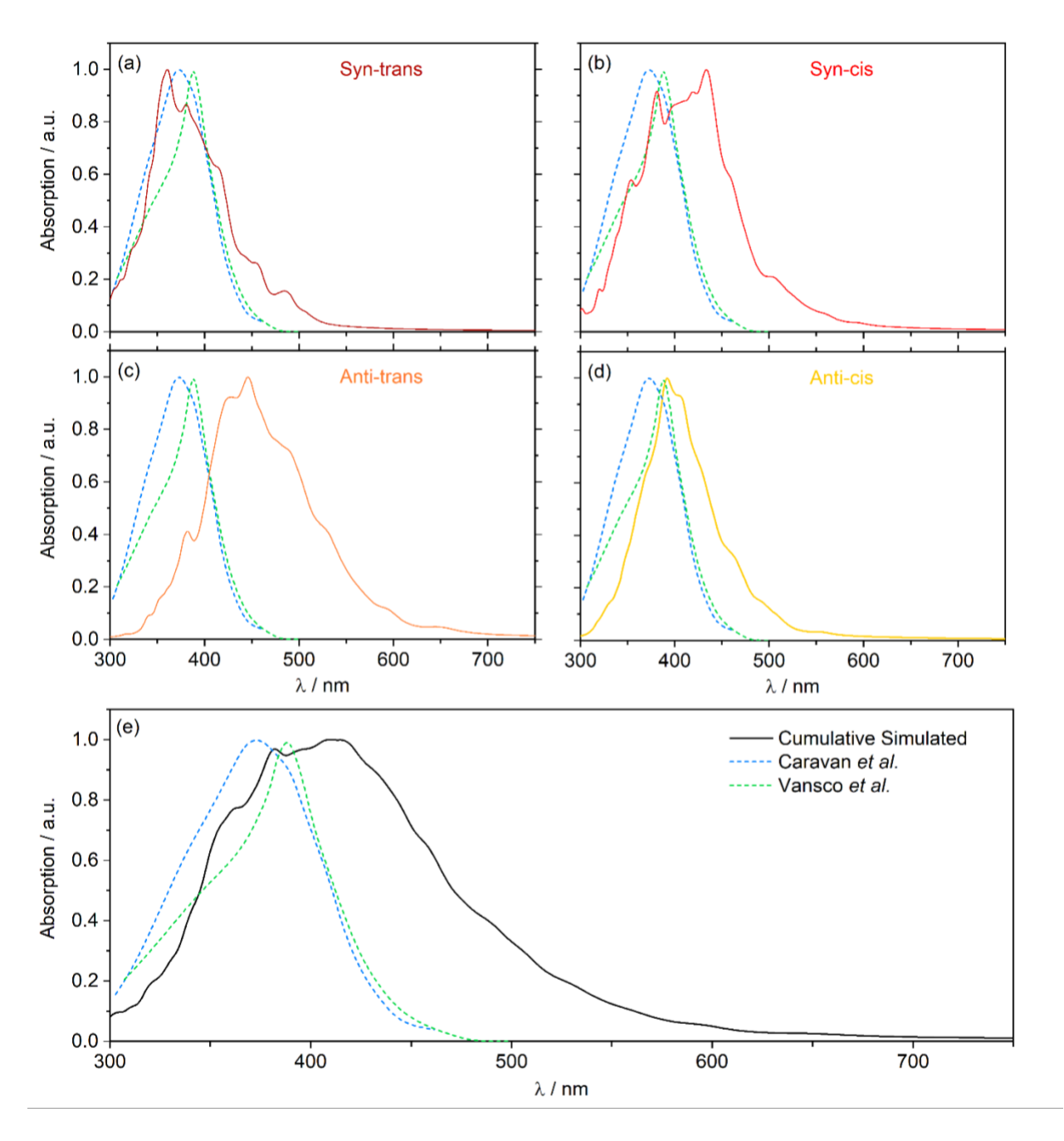


Figure 2: CASPT2 simulated electronic absorption profiles of the (a) ST, (b) SC, (c) AT and (d) AC conformers of MVK-oxide, as well as (e) the convoluted spectra of all four conformers. Plotted alongside are the experimental absorption spectra measured by Vansco et al. (green spectral profile)⁴⁶ and Caravan et al. (blue spectral profile)⁷¹

Table 1: Absolute calculated photoabsorption cross sections of the four conformers of MVK-oxide and MACR-oxide at the peak maximum. Alongside are the photolysis rate constants.

Criegee Intermediate	σ / 10 ⁻¹⁷ cm ²	Photolysis Rate Constant / s ⁻¹				
MVK-oxide Conformers						
syn-cis	1.04	0.57				
syn-trans	1.30	0.44				
anti-cis	0.96	0.38				
anti-trans	1.03	0.77				
MACR-oxide conformers						
syn-cis	0.59	0.22				
syn-trans	0.75	0.44				
anti-cis	0.63	0.55				
anti-trans	1.19	0.73				

The experimental electronic absorption spectra measured under jet-cooled (\sim 10 K), and thermalized (298 K) conditions show broad spectral profiles, ranging from 490 nm > λ_{phot} > 300 nm, with maxima centered at ca. 390 nm and 370 nm, respectively. Previous studies⁴⁶ show that this absorption band is attributable to a strongly absorbing $\pi\pi^*$ state, formed via a $\pi^* \leftarrow \pi$ orbital promotion, wherein the participating orbitals are centered on the carbonyl-oxide moiety. This is reinforced by our computations of the orbital promotions of the various electronic states in Figure S5 of the supporting information.

The populations of the four conformers of MVK-oxide likely do not follow a room temperature Boltzmann distribution in the measurements obtained under jet-cooled conditions, even though the conformers have varying stabilities as MVK-oxide is prepared in a non-statistical manner prior to chamber delivery. Therefore, it may be entirely possible that all conformers, including the least stable AC-conformer may be present. Indeed, the evidence of the presence of *anti* conformers was observed in recent experiments,^{70,71} although the relative populations of the various *syn* and *anti* conformers could not be determined. We will discuss the involvement of the various conformers later in the text.

The conformer-convoluted simulated absorption spectrum (Figure 2(e)) calculated using CASPT2(12/10), as well as the other two active spaces (given in the supporting information), shows a red shift in its absorption maxima when compared to the experimentally returned spectra and covers a broader wavelength range. Given this observation, we will first compare the absorption profiles of the individual conformers in the discussion of the performance of the three active spaces. We will however return to the implications of the disagreement of the convoluted spectra to that of the experimentally measured spectra.

As Figure 2 shows, the most stable ST conformer shows the best agreement with the experimentally measured spectra. In contrast, the AT conformer shows the poorest agreement with the experimentally measured spectra. The cumulative spectrum, wherein we assume equal contributions of all four conformers, is in gross disagreement with experiment when comparing the peak maximum and the width of the spectra profile – which may imply an unequal contribution from the four conformers. Given these details and that our previous studies on the simplest Criegee intermediate (CH₂OO) have shown good agreement at the CASPT2(12/10) level of theory, 49 we have analyzed the conformer-dependent intensity distributions of the four conformers of MVK-oxide by scaling the conformer intensities based on their respective Boltzmann populations at various temperatures. The large temperature range explored in this study (0 - 3000 K) was chosen primarily by considering the methodology used for the synthesis of the Criegee intermediates in laboratory studies and consequently the acquisition of their electronic spectra. The synthesis methodology is expected to lead to the formation of Criegee Intermediates with high internal energies (which exceed the barrier for interconversion between various conformers). Thus, when the Criegee intermediates are thermilized, the relative populations into different conformers may differ considerably from those expected on the basis

of Boltzmann distribution at 298 K. Figure 3 presents the conformer-dependent summed spectra of all four-conformers. The Boltzmann populations of the conformers at a given temperature are given in Table 2 – based on their relative minimum energies as calculated by Barber et al. 70 The spectra in Figure 3 are prepared by scaling the absolute energy-dependent photoabsorption cross sections (calculated from equation 1) associated with the individual conformers by their Boltzmann populations at the chosen temperature, but the Wigner distributions are not broadened by the assumed temperature. Therefore, Figure 3 simply illustrates the sensitivity of the calculated cumulative absorption spectrum to the mix of conformers. This is legitimate for comparison to the spectrum obtained under jet-cooled conditions since we are assuming that the conformer distributions at a given temperature represent the distributions before the molecules are introduced into the interaction volume of the experiment. This is a fair assumption since the calculated barriers to interconversion between the individual conformers are higher than the internal energy distribution imparted by the assumed temperature. ⁷⁰ As such the Boltzmann populations at a given temperature are conformationally locked and then cooled upon supersonic expansion.

As expected, Table 1 confirms that the ST conformer has the dominant contribution at low temperatures. At 3000 K, all four conformers are present with (an almost) equal contribution. As shown in Figure 3, the absorption spectral profile at low temperatures is in better agreement with experiment than at high temperatures. Guided by this spectrum, we speculate that, despite the MVK-oxide being prepared with high internal energy, the jet-cooled experimental electronic absorption spectrum (Figure 2, green spectral profile) is built upon starting conformer distributions that are close to a thermal Boltzmann distribution, wherein ST is the dominant conformer, and the three other conformers make minor contributions. This is a plausible

conclusion if the rotational barriers to interconversion between the conformers are above the internal energy distribution of each MVK-oxide conformer. We recognize however that a few considerations need to be made. Firstly, the calculated Boltzmann populations in Table 2 represent crude estimates, which may not reflect the actual conformer distributions under the set experimental conditions. In other words, population of higher energy conformers and consequently their contribution to the overall electronic spectrum may be higher than that predicted based on the Boltzmann analysis described above. In addition, our conclusion is based on assuming that the CASPT2(12/10) simulated spectra give the best agreement with experiment, which is reasonable given our previous work that shows that CASPT2(12/10) gives the best agreement with the experimentally measured absorption spectra of CH₂OO and CH₃CHOO.⁴⁹

Nevertheless, we conclude that the ST conformer contributes the most to the electronic absorption profiles which is consistent with experimentally measured time-resolved absorption spectra of MVK-oxide obtained under thermal conditions (Figure 2, blue spectral profile). The transient absorption time trace for MVK-oxide obtained at 298 K exhibits a slow decay that is consistent with the predicted rate coefficient for unimolecular decay of the *syn*-conformers of MVK-oxide, suggesting that *syn*-MVK-oxide is the dominant spectral carrier. The room temperature spectrum of MVK-oxide is therefore in good agreement with the simulated electronic absorption profile of *syn-trans*-MVK-oxide, which is expected to be the most populated conformer at 298 K (Table 2).

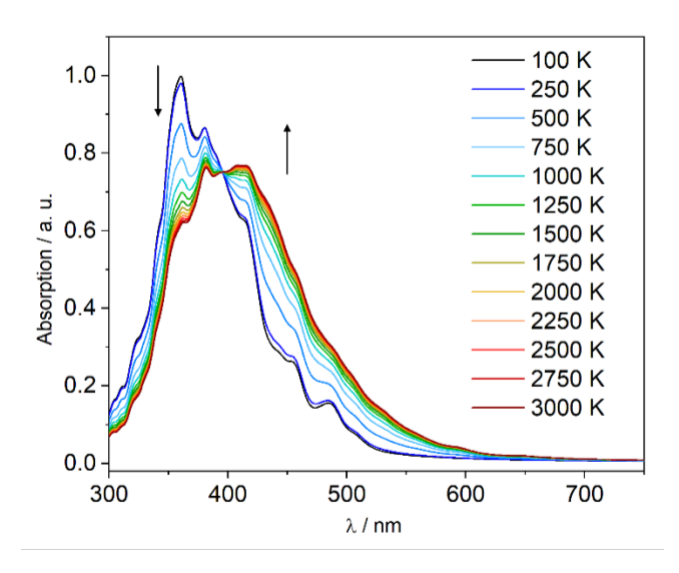


Figure 3: Summed absorption profiles of all four conformers as a function of temperature.

Table 2: Boltzmann populations of the four conformers of MVK-oxide at various temperatures. The calculated relative energies are 0 (ST), 1.76 (SC), 2.57 (AT) and 3.05 (AC) kcal/mol.⁷⁰

Temperature / K	AC	ST	AT	SC
100	0.00	1.00	0.00	0.00
250	0.00	0.96	0.01	0.03
500	0.04	0.77	0.06	0.13
750	0.08	0.62	0.11	0.19
1000	0.11	0.53	0.14	0.22
1250	0.14	0.47	0.17	0.23
1500	0.15	0.43	0.18	0.24
1750	0.17	0.40	0.19	0.24
2000	0.18	0.38	0.20	0.24
2250	0.18	0.36	0.21	0.25
2500	0.19	0.35	0.21	0.25
2750	0.20	0.34	0.21	0.25
3000	0.20	0.33	0.22	0.25

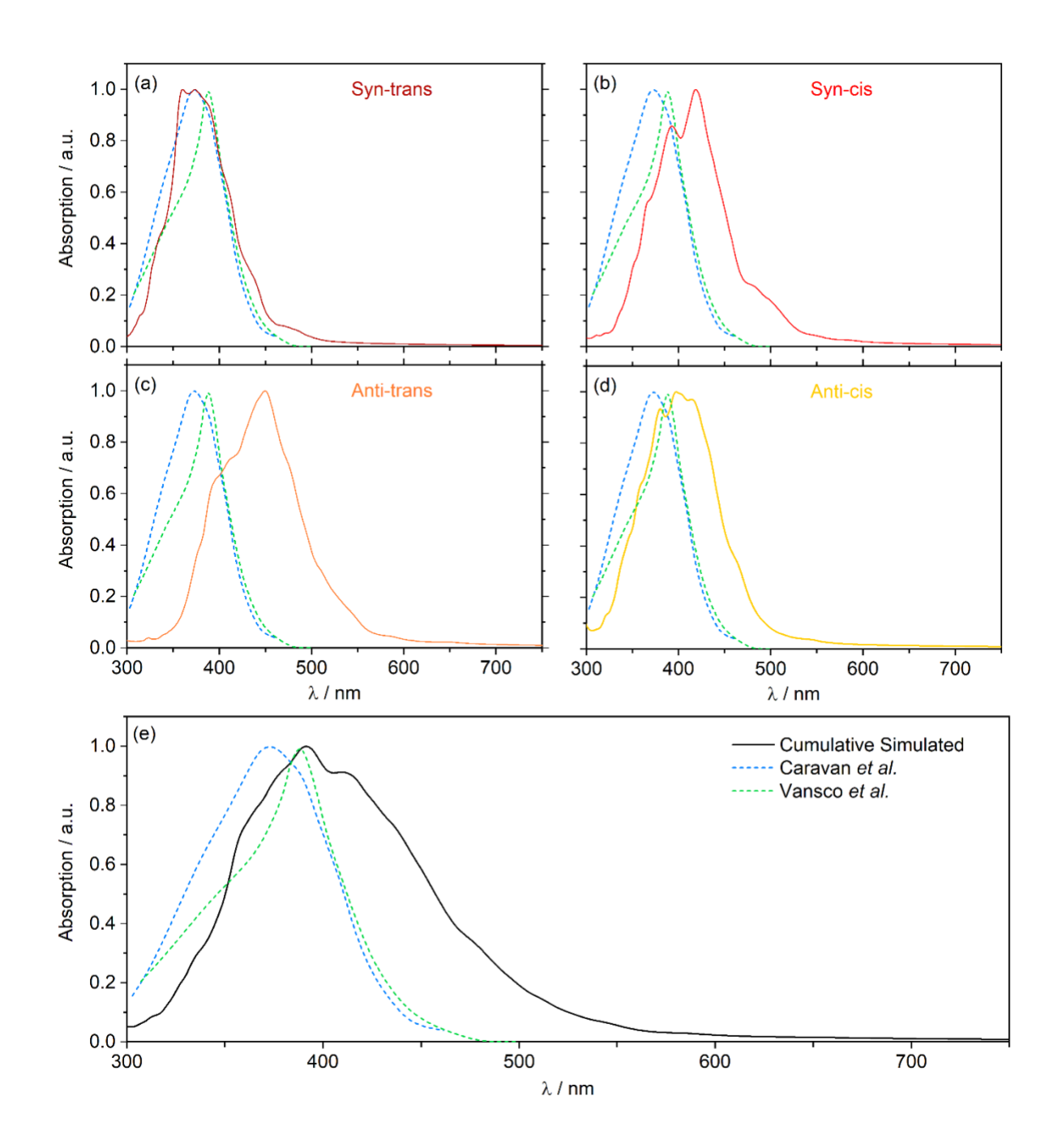


Figure 4: TDDFT simulated electronic absorption profiles of the (a) ST, (b) SC, (c) AT and (d) AC conformers of MVK-oxide, as well as (e) the convoluted spectra of all four conformers. Plotted alongside are the experimental absorption spectra measured by Vansco et al. (green spectral profile)⁴⁶ and Caravan et al. (blue spectral profile)⁷¹

For completion we have also simulated the electronic absorption spectrum of MVK-oxide using TD-DFT (TD-CAM-B3LYP/6-311+G(d,p)). The individual spectra of the conformers (panels (a) – (d)) and the cumulative spectrum are created in the same way as described above for the CASPT2 spectra of MVK-oxide.

In this and our previous study on CH₂OO and CH₃CHOO, we discovered that TD-CAM-B3LYP/6-311+G(d,p) systematically overestimates the peak position of the absorption profile. In that study we derived an energy shift factor (0.69 eV) so that the TDDFT simulated electronic absorption spectrum for CH₂OO matched the experimentally measured spectrum.⁴⁹ Applying this same shift factor to CH₃CHOO showed exceptional agreement between the shifted TDDFT and measured spectra for CH₃CHOO. Here, we use the same energy shift factor derived for CH₂OO to shift the simulated TDDFT spectrum for MVK-oxide; the returned spectra are given in Figure 4 while the unshifted raw spectra are displayed Figure S7. The shifted TDDFT (TD-CAM-B3LYP/6-311+G(d,p)) spectra are in excellent agreement with the CASPT2 spectra when comparing the peak position, profile topology and spectral width. This observation is reassuring and a confirmation that the original energy shift factor derived from the simplest Criegee Intermediate, CH₂OO, may be systematically used to larger and more complex Criegee Intermediates wherein CASPT2 becomes computationally restrictive.

Electronic absorption spectrum of MACR-oxide

Figure 1(b) depicts the ground state minimum energy geometry of the four lowest-energy conformers of MACR-oxide. *Syn* and *anti* are distinguishable by whether the terminal oxygen atom of the carbonyl-oxide moiety is orientated, respectively, towards or away from the terminal carbon atom of the alkene moiety. *Cis* and *trans* describe the relative orientation of the alkene moiety and whether it is orientated towards or away from the carbonyl-oxide moiety,

respectively. The relative stabilities of the four conformers of MACR-oxide are as follows: AT > SC > ST > AC.⁴⁷

Figure 4 displays the CASPT2(12/10) calculated electronic absorption profiles of the (a) ST, (b) SC, (c) AT and (d) AC conformers of MACR-oxide alongside the cumulative simulated spectrum (e). The experimental electronic absorption spectra, measured by Vansco *et al.* under jet-cooled conditions (green spectral profile)⁴⁷ and Lin *et al.* under thermal conditions (298 K, blue spectral profile)⁷⁴ is plotted alongside each simulated spectrum. The additional CASPT2(10/8) and CASPT2(8/6) calculated electronic absorption profiles can be found in supporting information (Figures S1 and S2). Again, the peak maxima associated with the individual conformers (panels (a) – (d)) are normalized to match that of the experimentally measured spectra. The cumulative spectrum is created in the same way as described above for the CASPT2 spectra of MVK-oxide.

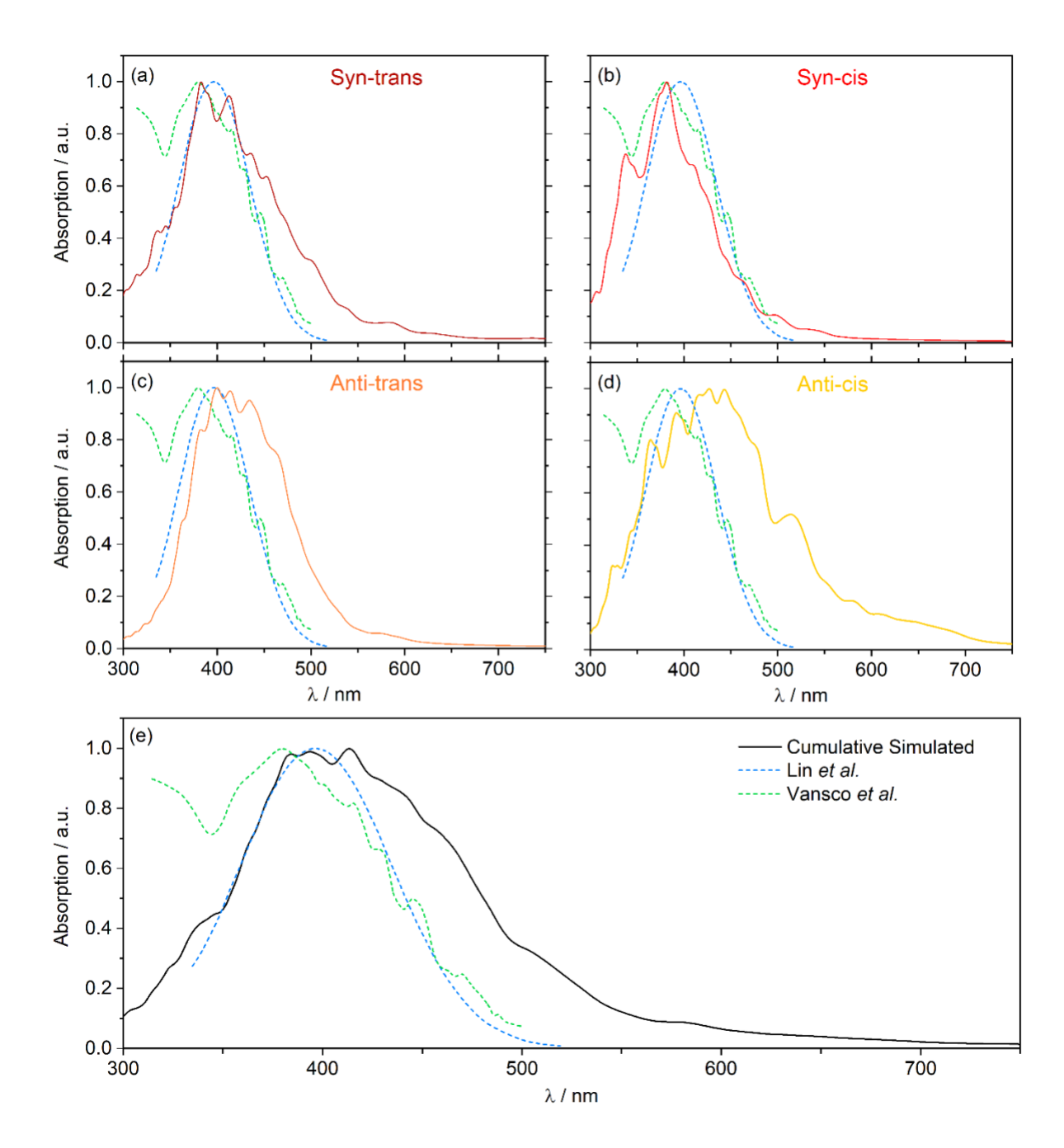


Figure 5: CASPT2 simulated electronic absorption profiles of the (a) ST, (b) SC, (c) AT and (d) AC conformers of MACR-oxide, as well as (e) the convoluted spectra of all four conformers. The experimental electronic absorption spectra, measured by Vansco *et al.* (green spectral profile)⁴⁷ and Lin *et al.* (blue spectral profile),⁷⁴ are plotted alongside each simulated spectrum

The experimental electronic absorption spectra measured by Vansco et al. and Lin et al. range from 500 nm to ca. 350 nm with a peak maximum of ca. 390 nm. Previous literature on the UV absorption profile of MACR-oxide show that this absorption band is formed via electronic excitation to a strongly absorbing $\pi\pi^*$ state, formed via a $\pi^* \leftarrow \pi$ orbital promotion, wherein the participating orbitals are both localized on the carbonyl-oxide functional group. As with MVKoxide, we note that the four conformers of MACR-oxide have varying stabilities. Therefore, for the experiments conducted under jet-cooled conditions the population into the various conformer minima are again not expected to follow a thermal Boltzmann distribution as the MACR-oxide is expected to form in a non-equilibrium distribution of conformers prior to supersonic expansion. As with MVK-oxide, the cumulative simulated electronic absorption spectrum of all fourconformers of MACR-oxide (displayed in Figure 4(e)) – assuming equal conformer populations - shows a red shift when compared to the experimentally measured spectra. Since the peak maxima are predominantly $\pi\pi^*$ in character, the peak positions are clear consequences of the differences in the π and π^* orbital stabilities of each conformer. In this case, ST and AT show the best agreement with the experimentally measured spectra and both have the highest absorption cross sections at the peak maximum – as shown in Table 1. AC and SC show the poorest agreement with experiment but also exhibit the lowest photoabsorption cross sections. The cumulative absorption spectrum in Figure 4(e), which captures the effects of the photoabsorption cross sections (but assumes an equal conformer distribution) is broader than the experimentally determined absorption spectra. Notwithstanding, the peak position agrees better with the experiment than the equivalent peak position in MVK-oxide.

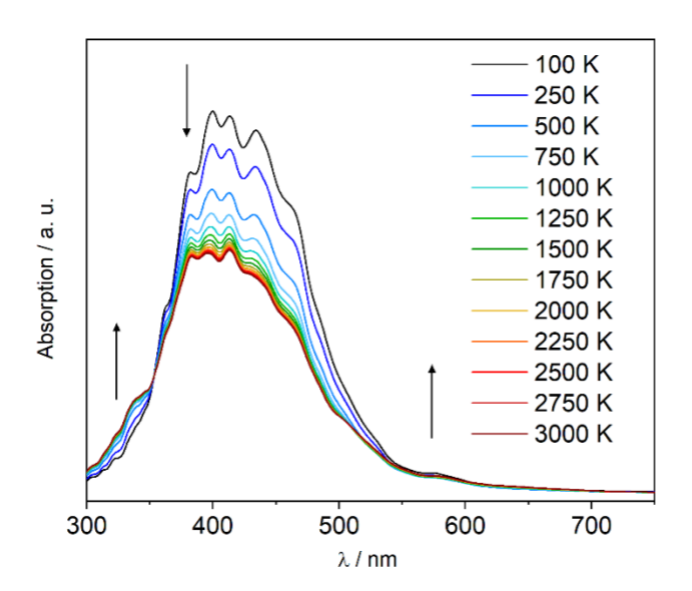


Figure 6: Summed absorption profiles of all four conformers of MACR-oxide as a function of temperature.

Table 3: Boltzmann populations of the four conformers of MACR-oxide at various temperatures. The calculated relative energies are 2.5 (ST), 0.91 (SC), 0 (AT) and 3.18 (AC) kcal/mol.⁴⁷

Temperature / K	AC	ST	AT	SC
100	0.00	0.00	0.99	0.01
250	0.00	0.01	0.86	0.14
500	0.03	0.05	0.66	0.26
750	0.06	0.10	0.54	0.29
1000	0.10	0.13	0.47	0.30
1250	0.12	0.16	0.43	0.30
1500	0.14	0.17	0.40	0.29
1750	0.15	0.18	0.38	0.29
2000	0.16	0.19	0.36	0.29
2250	0.17	0.20	0.35	0.28
2500	0.18	0.20	0.34	0.28
2750	0.18	0.21	0.33	0.28
3000	0.19	0.21	0.32	0.28

Given the aforementioned, we have computed the conformer-dependent intensity distributions of the four conformers of MACR-oxide by scaling the photoabsorption cross section profiles of each conformer based on their respective Boltzmann populations at various temperatures. Figure 6 displays the returned cumulative spectrum of all four-conformers at various Boltzmann temperatures. These spectra are calculated in the same way as those derived for MVK-oxide. The Boltzmann populations of the conformers at a given temperature are given in Table 3, based on minimum energy calculations by Vansco et al. 47 With no surprise, Table 3 confirms that the AT conformer has the dominant contribution at low temperatures. At 3000 K, all four conformers are present with almost equal Boltzmann populations compared to their relative stabilities. Since all conformers show almost equivalent peak maxima, it is not possible to unambiguously imply conformer contributions as was done in MVK-oxide. Despite this, the overall shape and amplitude of this conformer-dependent spectra are noteworthy. As a reminder, the stabilities of the conformers are ordered: AT > SC > ST > AC, whilst Table 1 shows that the photoabsorption cross sections are ordered: AT >> AC~ST > SC. As Table 3 implies the AT conformer will dominate at all temperatures and thus the profile is relatively insensitive to the temperature – with some narrowing of the profile upon decreasing temperature that matches the profile of the AT conformer in Figure 4(c). Notably, the absolute amplitude falls upon increasing temperature since the AT conformer contribution decreases. The increasing contribution of the SC conformer at higher temperatures is revealed by the increase in the predicted absorbance at $\lambda \sim 330$ nm (Figure 6, black arrows). The increased contributions of both the AC and ST conformers upon increasing temperature are revealed by the (relative) persistence of absorption at $\lambda > 500$ nm.

Similar to that observed for MVK-oxide, the transient absorption time trace for MACR-oxide obtained under thermal conditions (298 K) exhibits a slow decay (ca. 3 ms)⁷⁴ that is significantly longer than the predicted unimolecular decomposition rate of the *syn* conformers of MACR-oxide (< 0.4 ms).⁷⁵ Therefore, the thermal spectrum is attributed to *anti*-MACR-oxide,

and consistent with the simulated electronic absorption profile of *anti-trans*-MACR-oxide in this work, which is expected to be the most populated conformer at 298 K (Table 3).

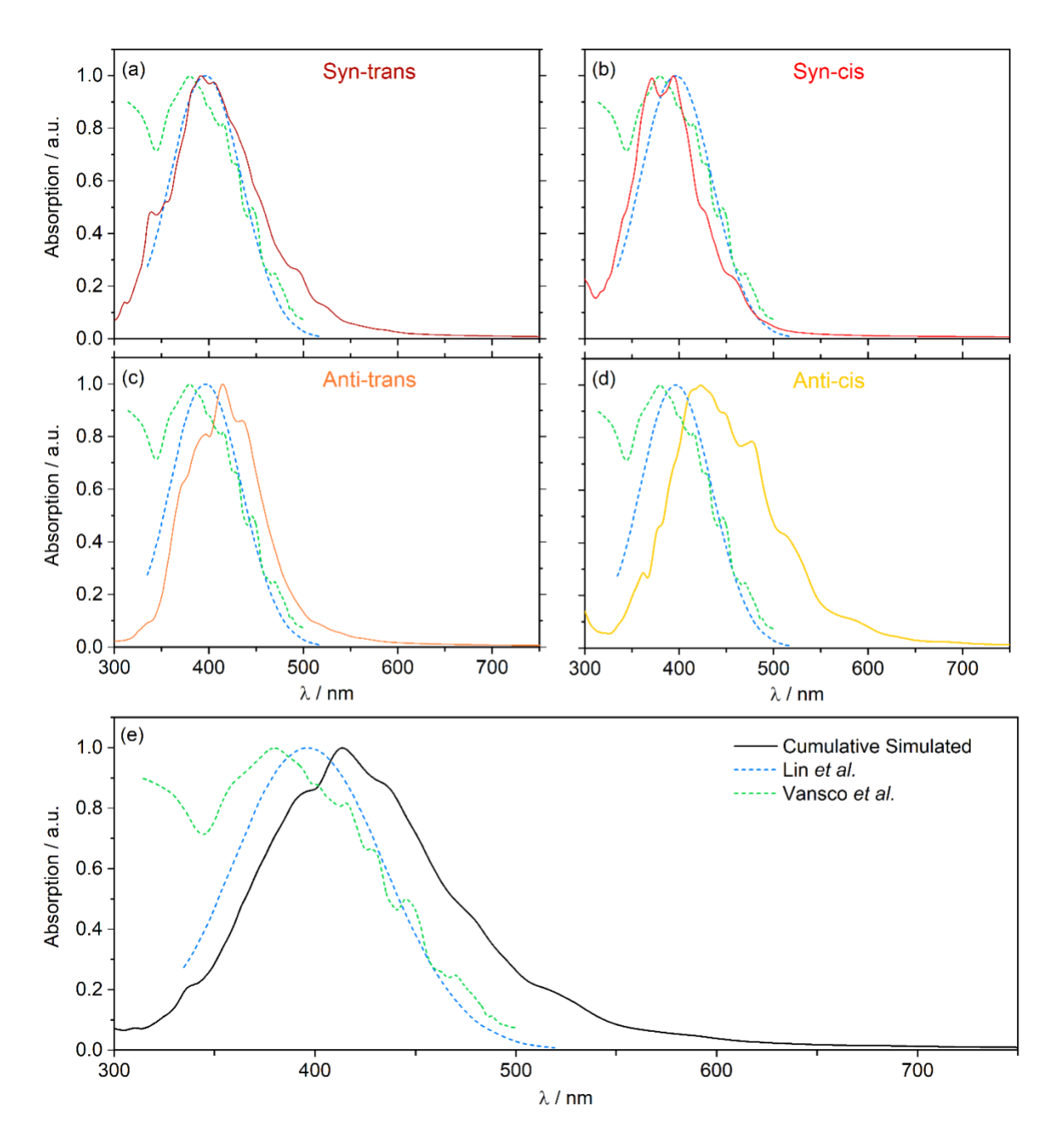


Figure 7: TDDFT simulated electronic absorption profiles of the (a) ST, (b) SC, (c) AT and (d) AC conformers of MACR-oxide, as well as (e) the convoluted spectra of all four conformers.

The experimental electronic absorption spectra, measured by Vansco *et al.* (green spectral profile)⁴⁷ and Lin *et al.* (blue spectral profile),⁷⁴ are plotted alongside each simulated spectrum.

Again, for completion we have also simulated the electronic absorption spectrum of MACR-oxide using TD-DFT (TD-CAM-B3LYP/aug-cc-pVDZ) using the energy shift factor (0.69 eV) derived for CH₂OO (as described above).⁴⁹ We apply this same energy shift factor derived for CH₂OO to shift the simulated TDDFT spectra of MACR-oxide; the returned spectra are given in Figure 4 while the unshifted raw spectra are displaced Figure S7. The shifted TDDFT spectra are in excellent agreement with the CASPT2 spectra and, again, reassures us that the original energy shift factor derived from the simplest Criegee Intermediate may be used to larger and more complex Criegee Intermediates wherein CASPT2 becomes computationally restrictive.

Conclusions

In this manuscript we sought to model the conformer specific electronic absorption spectra of two classes of large Criegee Intermediate, MVK-oxide and MACR-oxide. Conformer contributions are varied by changing the temperature within the Boltzmann relation, wherein temperature is merely a population varying parameter and not an implied temperature at which the spectra are measured. Using this approach, we have shown that in MVK-oxide, assuming an equal contribution of conformers leads to a significant mismatch between the simulated and experimentally measured spectra. By judiciously varying the conformer populations, we are able to qualitatively imply relative contributions of the various conformers to the experimentally measured absorption spectra wherein the most stable ST conformer was shown to have the greatest contribution to the absorption profile.

The conformer contribution to the electronic absorption spectrum of MACR-oxide was less clear cut, owing to the smaller differences in the peak absorption wavelengths between the four conformers. In this case however, differences in the absolute photoabsorption cross sections of the individual conformers lead to marked and obvious changes in the peak intensity upon variation of the conformer distribution. A future experimental measurement of the peak photoabsorption cross section of MACR-oxide would allow for determination of the conformer distribution reported herein. Such a value is however hitherto unreported, to the best of our knowledge. Estimated photolysis rates for all four conformers of both MVK-oxide and MACR-oxide are faster than the experimentally measured values for CH₂OO and CH₃CHOO, implying that solar photolysis may become a competitive removal path for MVK-oxide and MACR-oxide. Specifically, the solar photolysis rates calculated for the most stable conformers of MVK-oxide (syn-trans, 0.44 s⁻¹) and MACR-oxide (anti-trans, 0.73 s⁻¹) are 3-5 times faster than those calculated for formaldehydeoxide (CH₂OO, 0.16 s⁻¹) and acetaldehyde-oxide (CH₃CHOO, 0.14 s⁻¹). ³¹ The increased photolysis rates for MVK-oxide and MACR-oxide is due to the bathochromic shift in their absorption spectra to a region of the solar spectrum that has better overlap with the actinic flux. As such, the larger photolysis rates for MVK-oxide and MACR-oxide compared to CH₂OO suggests solar photolysis plays a more prominent role in the atmospheric removal of the four-carbon unsaturated Criegee intermediates from isoprene ozonolysis. However, comparison with other decay pathways available to the Criegee intermediates should be taken into account. Thermalized Criegee intermediates have several potential removal pathways in the atmosphere including bimolecular reaction with water vapor, organic acids and SO₂, as well as unimolecular decomposition.^{23,76} The primary removal pathway for CH₂OO is expected to be reaction with water dimer. However, it has been recently demonstrated that MVK-oxide and MACR-oxide react with water vapor on

significantly longer timescale *cf.* CH₂OO due to a combination of steric hindrance and disruption of their extended conjugation upon reaction.^{23,71,74} Therefore, other loss pathways can compete for the removal of MVK-oxide and MACR-oxide in the atmosphere. By evaluating the effective loss rates of syn-MVK-oxide and anti-MACR-oxide under tropospheric conditions predicted for the Amazon region (e.g. bimolecular reaction with water vapor, SO2, formic acid and acetic acid, and unimolecular decomposition),^{71,74–77} we estimate that solar photolysis plays a minor, but non-negligible role in the removal of syn-MVK-oxide and anti-MACR-oxide (~1%).

Although the nuclear ensemble method contains shortcomings, as noted by us⁴⁹ and others^{78–80} before, it is a simple method that allows for a swift qualitative description of the electronic absorption profile of a given system. As we have shown in this contribution and before⁴⁹, the choice of the electronic structure method is a key factor that needs to be considered carefully, both in the computation of the electronic absorption spectrum at hand, and its feasibility of extension to larger systems. Moving forward we hope to extend the current systems to Criegee Intermediates of further increased molecular complexity – particularly those formed by the ozonolysis of endocyclic alkenes such as α -pinene and β -caryophyllene. For such Criegee Intermediates, we are particularly looking forward to using the recently developed machine learning nuclear ensemble method.⁸¹

Acknowledgements

The work reported in this manuscript is supported by the National Science Foundation, under grant no. 2003422. This material is based in part on research at Argonne supported by the U.S. Department of Energy, Office of Science, Office of Basic Energy Sciences, Division of Chemical Sciences, Geosciences, and Biosciences under Contract No. DE-AC02-06CH11357. We also thank Professor Michael Ashfold (University of Bristol) for fruitful discussions.

Supporting Information

Example fit to $F(\lambda)$, used to derive the photolysis rates; Simulated CASPT2(10/8) spectra for MVK-oxide and MACR-oxide; Simulated CASPT2(8/6) spectra for (a) MVK-oxide and (b) MACR-oxide; Active orbitals for the CASSCF(12/10)/CASPT2(12/10) calculations for (a) MVK-oxide and (b) MACR-oxide; vertical excitation energies, oscillator strengths and predominant orbital excitations of the 1 n π *, 1 $\pi\pi$ * and 2 $\pi\pi$ * states of the four conformers of MVK-oxide; vertical excitation energies, oscillator strengths and predominant orbital excitations of the 1 n π *, 1 $\pi\pi$ * and 2 $\pi\pi$ * states of the four conformers of MACR-oxide; B3LYP/6-311+G(d,p) optimized geometries of the four conformers of MVK-oxide; B3LYP/6-311+G(d,p) optimized geometries of the four conformers of MACR-oxide; Simulated CASPT2(12/1)/AVDZ spectra for syn-trans-MVK-oxide using different Lorentzian broadening factors; Optimized parameters of the four conformers of MVK-oxide and MACR-oxide using B2PLYP-D3, B3LYP and MP2; Normal mode wavenumbers of the four conformers of MVK-oxide and MACR-oxide using B2PLYP-D3, B3LYP and MP2; Vertical excitation energies (in eV) of syn-trans-MVK-oxide and anti-trans-MACR-oxide calculated at CASPT2(14/11)/AVDZ and

CASPT2(16/10)/AVDZ; Vertical excitation energies (in eV) of CASPT2(12/10)/AVDZ optmised geometry of syn-trans-MVK-oxide and anti-trans-MACR-oxide calculated at CASPT2(12/10)/AVDZ.

The authors declare no conflicts of interest

References

- (1) Stone, D.; Whalley, L. K.; Heard, D. E. Tropospheric OH and HO2 Radicals: Field Measurements and Model Comparisons. *Chem. Soc. Rev.* **2012**, *41* (19), 6348–6404. https://doi.org/10.1039/C2CS35140D.
- (2) Finlayson, B. J.; Pitts, J. N. *Chemistry of the Upper and Lower Atmosphere*; Academic Press: San Diego, 2000.
- (3) Harrison, R. M.; Yin, J.; Tilling, R. M.; Cai, X.; Seakins, P. W.; Hopkins, J. R.; Lansley, D. L.; Lewis, A. C.; Hunter, M. C.; Heard, D. E.; Carpenter, L. J.; Creasey, D. J.; Lee, J. D.; Pilling, M. J.; Carslaw, N.; Emmerson, K. M.; Redington, A.; Derwent, R. G.; Ryall, D.; Mills, G.; Penkett, S. A. Measurement and Modelling of Air Pollution and Atmospheric Chemistry in the U.K. West Midlands Conurbation: Overview of the PUMA Consortium Project. *Sci. Total Environ.* 2006, 360 (1), 5–25. https://doi.org/https://doi.org/10.1016/j.scitotenv.2005.08.053.
- (4) Fang, Y.; Liu, F.; Barber, V. P.; Klippenstein, S. J.; McCoy, A. B.; Lester, M. I. Communication: Real Time Observation of Unimolecular Decay of Criegee Intermediates to OH Radical Products. *J. Chem. Phys.* 2016, 144 (6), 61102.

- https://doi.org/10.1063/1.4941768.
- (5) Gligorovski, S.; Strekowski, R.; Barbati, S.; Vione, D. Environmental Implications of Hydroxyl Radicals (•OH). *Chem. Rev.* **2015**, *115* (24), 13051–13092. https://doi.org/10.1021/cr500310b.
- (6) Alam, M. S.; Camredon, M.; Rickard, A. R.; Carr, T.; Wyche, K. P.; Hornsby, K. E.; Monks, P. S.; Bloss, W. J. Total Radical Yields from Tropospheric Ethene Ozonolysis. *Phys. Chem. Chem. Phys.* 2011, *13* (23), 11002–11015. https://doi.org/10.1039/C0CP02342F.
- (7) Donahue, N. M.; Drozd, G. T.; Epstein, S. A.; Presto, A. A.; Kroll, J. H. Adventures in Ozoneland: Down the Rabbit-Hole. *Phys. Chem. Chem. Phys.* **2011**, *13* (23), 10848–10857. https://doi.org/10.1039/C0CP02564J.
- (8) Novelli, A.; Vereecken, L.; Lelieveld, J.; Harder, H. Direct Observation of OH Formation from Stabilised Criegee Intermediates. *Phys. Chem. Chem. Phys.* **2014**, *16* (37), 19941–19951. https://doi.org/10.1039/C4CP02719A.
- (9) Kroll, J. H.; Clarke, J. S.; Donahue, N. M.; Anderson, J. G. Mechanism of HOx Formation in the Gas-Phase Ozone–Alkene Reaction. 1. Direct, Pressure-Dependent Measurements of Prompt OH Yields. *J. Phys. Chem. A* 2001, 105 (9), 1554–1560. https://doi.org/10.1021/jp002121r.
- (10) Huang, H. L.; Chao, W.; Lin, J. J. M. Kinetics of a Criegee Intermediate That Would Survive High Humidity and May Oxidize Atmospheric SO2. *Proc. Natl. Acad. Sci. U. S. A.* **2015**, *112* (35), 10857–10862. https://doi.org/10.1073/pnas.1513149112.
- (11) Osborn, D. L.; Taatjes, C. A. The Physical Chemistry of Criegee Intermediates in the Gas Phase. *Int. Rev. Phys. Chem.* **2015**, *34* (3), 309–360.

- https://doi.org/10.1080/0144235X.2015.1055676.
- (12) Chhantyal-Pun, R.; Khan, M. A. H.; Martin, R.; Zachhuber, N.; Buras, Z. J.; Percival, C. J.; Shallcross, D. E.; Orr-Ewing, A. J. Direct Kinetic and Atmospheric Modeling Studies of Criegee Intermediate Reactions with Acetone. *ACS Earth Sp. Chem.* 2019. https://doi.org/10.1021/acsearthspacechem.9b00213.
- (13) Johnson, D.; Marston, G. The Gas-Phase Ozonolysis of Unsaturated Volatile Organic Compounds in the Troposphere. *Chem. Soc. Rev.* **2008**, *37* (4), 699–716. https://doi.org/10.1039/B704260B.
- (14) Emmerson, K. M.; Carslaw, N. Night-Time Radical Chemistry during the TORCH Campaign. *Atmos. Environ.* 2009, 43 (20), 3220–3226.
 https://doi.org/https://doi.org/10.1016/j.atmosenv.2009.03.042.
- (15) Emmerson, K. M.; Carslaw, N.; Carslaw, D. C.; Lee, J. D.; McFiggans, G.; Bloss, W. J.; Gravestock, T.; Heard, D. E.; Hopkins, J.; Ingham, T.; Pilling, M. J.; Smith, S. C.; Jacob, M.; Monks, P. S. Free Radical Modelling Studies during the UK TORCH Campaign in Summer 2003. *Atmos. Chem. Phys.* 2007, 7 (1), 167–181. https://doi.org/10.5194/acp-7-167-2007.
- (16) Alam, M. S.; Rickard, A. R.; Camredon, M.; Wyche, K. P.; Carr, T.; Hornsby, K. E.; Monks, P. S.; Bloss, W. J. Radical Product Yields from the Ozonolysis of Short Chain Alkenes under Atmospheric Boundary Layer Conditions. *J. Phys. Chem. A* 2013, *117* (47), 12468–12483. https://doi.org/10.1021/jp408745h.
- (17) Hasson, A. S.; Orzechowska, G.; Paulson, S. E. Production of Stabilized Criegee Intermediates and Peroxides in the Gas Phase Ozonolysis of Alkenes: 1. Ethene, Trans-2-Butene, and 2,3-Dimethyl-2-Butene. *J. Geophys. Res. Atmos.* 2001, 106 (D24), 34131–

- 34142. https://doi.org/10.1029/2001JD000597.
- (18) Meidan, D.; Holloway, J. S.; Edwards, P. M.; Dubé, W. P.; Middlebrook, A. M.; Liao, J.; Welti, A.; Graus, M.; Warneke, C.; Ryerson, T. B.; Pollack, I. B.; Brown, S. S.; Rudich, Y. Role of Criegee Intermediates in Secondary Sulfate Aerosol Formation in Nocturnal Power Plant Plumes in the Southeast US. ACS Earth Sp. Chem. 2019, 3 (5), 748–759. https://doi.org/10.1021/acsearthspacechem.8b00215.
- (19) Criegee Mechanism of Ozonolysis BT Name Reactions: A Collection of Detailed Reaction Mechanisms; Li, J. J., Ed.; Springer Berlin Heidelberg: Berlin, Heidelberg, 2014. https://doi.org/10.1007/3-540-30031-7_77.
- (20) Criegee, R. Mechanism of Ozonolysis. *Angew. Chemie Int. Ed. English* **2018**, *14* (11), 745–752. https://doi.org/10.1002/anie.197507451.
- (21) Geletneky, C.; Berger, S. The Mechanism of Ozonolysis Revisited by 17O-NMR Spectroscopy. *European J. Org. Chem.* 1998, 1998 (8), 1625–1627. https://doi.org/10.1002/(SICI)1099-0690(199808)1998:8<1625::AID-EJOC1625>3.0.CO;2-L.
- (22) Horie, O.; Moortgat, G. K. Gas-Phase Ozonolysis of Alkenes. Recent Advances in Mechanistic Investigations. *Acc. Chem. Res.* 1998, 31 (7), 387–396. https://doi.org/10.1021/ar9702740.
- (23) Khan, M. A. H.; Percival, C. J.; Caravan, R. L.; Taatjes, C. A.; Shallcross, D. E. Criegee Intermediates and Their Impacts on the Troposphere. *Environ. Sci. Process. Impacts* **2018**, 20 (3), 437–453. https://doi.org/10.1039/C7EM00585G.
- (24) Stephenson, T. A.; Lester, M. I. Unimolecular Decay Dynamics of Criegee Intermediates: Energy-Resolved Rates, Thermal Rates, and Their Atmospheric Impact. *Int. Rev. Phys.*

- Chem. 2020, 39 (1), 1–33. https://doi.org/10.1080/0144235X.2020.1688530.
- (25) Hansen, A. S.; Liu, Z.; Chen, S.; Schumer, M. G.; Walsh, P. J.; Lester, M. I. Unraveling Conformer-Specific Sources of Hydroxyl Radical Production from an Isoprene-Derived Criegee Intermediate by Deuteration. *J. Phys. Chem. A* **2020**, *124* (24), 4929–4938. https://doi.org/10.1021/acs.jpca.0c02867.
- (26) Mauldin III, R. L.; Berndt, T.; Sipilä, M.; Paasonen, P.; Petäjä, T.; Kim, S.; Kurtén, T.; Stratmann, F.; Kerminen, V.-M.; Kulmala, M. A New Atmospherically Relevant Oxidant of Sulphur Dioxide. *Nature* **2012**, *488*, 193.
- (27) Ting, A. W. L.; Lin, J. J. M. UV Spectrum of the Simplest Deuterated Criegee Intermediate CD2OO. J. Chinese Chem. Soc. 2017, 64 (4), 360–368. https://doi.org/10.1002/jccs.201700049.
- (28) Chang, Y. P.; Li, Y. L.; Liu, M. L.; Ou, T. C.; Lin, J. J. M. Absolute Infrared Absorption Cross Section of the Simplest Criegee Intermediate Near 1285.7 Cm-1. *J. Phys. Chem. A* **2018**, *122* (45), 8874–8881. https://doi.org/10.1021/acs.jpca.8b06759.
- (29) Foreman, E. S.; Kapnas, K. M.; Jou, Y. T.; Kalinowski, J.; Feng, D.; Gerber, R. B.; Murray, C. High Resolution Absolute Absorption Cross Sections of the B1A'-X1A' Transition of the CH2OO Biradical. *Phys. Chem. Chem. Phys.* 2015, *17* (48), 32539–32546. https://doi.org/10.1039/c5cp04977f.
- (30) Ting, W. L.; Chen, Y. H.; Chao, W.; Smith, M. C.; Lin, J. J. M. The UV Absorption Spectrum of the Simplest Criegee Intermediate CH 2OO. *Phys. Chem. Chem. Phys.* **2014**, *16* (22), 10438–10443. https://doi.org/10.1039/c4cp00877d.
- (31) Smith, M. C.; Ting, W. L.; Chang, C. H.; Takahashi, K.; Boering, K. A.; Lin, J. J. M. UV Absorption Spectrum of the C2 Criegee Intermediate CH3CHOO. *J. Chem. Phys.* **2014**,

- 141 (7), 074302. https://doi.org/10.1063/1.4892582.
- (32) Chang, Y.-P.; Chang, C.-H.; Takahashi, K.; Lin, J. J.-M. Absolute UV Absorption Cross Sections of Dimethyl Substituted Criegee Intermediate (CH3)2COO. *Chem. Phys. Lett.* 2016, 653, 155–160. https://doi.org/https://doi.org/10.1016/j.cplett.2016.04.082.
- (33) Sheps, L.; Scully, A. M.; Au, K. UV Absorption Probing of the Conformer-Dependent Reactivity of a Criegee Intermediate CH3CHOO. *Phys. Chem. Chem. Phys.* **2014**, *16* (48), 26701–26706. https://doi.org/10.1039/C4CP04408H.
- (34) Sheps, L. Absolute Ultraviolet Absorption Spectrum of a Criegee Intermediate CH 2OO. *J. Phys. Chem. Lett.* **2013**, *4* (24), 4201–4205. https://doi.org/10.1021/jz402191w.
- (35) Sršeň; Hollas, D.; Slavíček, P. UV Absorption of Criegee Intermediates: Quantitative Cross Sections from High-Level: Ab Initio Theory. *Phys. Chem. Chem. Phys.* **2018**, *20* (9), 6421–6430. https://doi.org/10.1039/c8cp00199e.
- (36) Dawes, R.; Jiang, B.; Guo, H. UV Absorption Spectrum and Photodissociation Channels of the Simplest Criegee Intermediate (CH2OO). *J. Am. Chem. Soc.* **2015**, *137* (1), 50–53. https://doi.org/10.1021/ja510736d.
- (37) Aplincourt, P.; Henon, E.; Bohr, F.; Ruiz-López, M. F. Theoretical Study of Photochemical Processes Involving Singlet Excited States of Formaldehyde Carbonyl Oxide in the Atmosphere. *Chem. Phys.* 2002, 285 (2–3), 221–231. https://doi.org/10.1016/S0301-0104(02)00804-2.
- (38) Ting, A. W.-L.; Lin, J. J.-M. UV Spectrum of the Simplest Deuterated Criegee Intermediate CD2OO. *J. Chinese Chem. Soc.* **2017**, *64* (4), 360–368. https://doi.org/10.1002/jccs.201700049.
- (39) Liu, F.; Beames, J. M.; Green, A. M.; Lester, M. I. UV Spectroscopic Characterization of

- Dimethyl- and Ethyl-Substituted Carbonyl Oxides. *J. Phys. Chem. A* **2014**, *118* (12), 2298–2306. https://doi.org/10.1021/jp412726z.
- (40) Beames, J. M.; Liu, F.; Lu, L.; Lester, M. I. UV Spectroscopic Characterization of an Alkyl Substituted Criegee Intermediate CH3CHOO. *J. Chem. Phys.* **2013**, *138* (24), 244307. https://doi.org/10.1063/1.4810865.
- (41) Kalinowski, J.; Foreman, E. S.; Kapnas, K. M.; Murray, C.; Räsänen, M.; Benny Gerber,
 R. Dynamics and Spectroscopy of CH2OO Excited Electronic States. *Phys. Chem. Chem. Phys.* 2016, *18* (16), 10941–10946. https://doi.org/10.1039/C6CP00807K.
- (42) Beames, J. M.; Liu, F.; Lu, L.; Lester, M. I. Ultraviolet Spectrum and Photochemistry of the Simplest Criegee Intermediate CH2OO. *J. Am. Chem. Soc.* **2012**, *134* (49), 20045–20048. https://doi.org/10.1021/ja310603j.
- (43) Anglada, J. M.; González, J.; Torrent-Sucarrat, M. Effects of the Substituents on the Reactivity of Carbonyl Oxides. A Theoretical Study on the Reaction of Substituted Carbonyl Oxides with Water. *Phys. Chem. Chem. Phys.* 2011, *13* (28), 13034–13045. https://doi.org/10.1039/C1CP20872A.
- Caravan, R. L.; Vansco, M. F.; Au, K.; Khan, A. A. H.; Li, Y. L.; Winiberg, F. A. F.;
 Zuraski, K.; Lin, Y. H.; Chao, W.; Trongsiriwat, N.; Walsh, P. J.; Osborn, D. L.; Percival,
 C. J.; Lin, J. M.; Shallcross, D. E.; Sheps, L.; Klippenstein, S. J.; Taatjes, C. A.; Lester, M.
 I. Direct Kinetic Measurements and Theoretical Predictions of an Isoprene-Derived
 Criegee Intermediate. *Proc. Natl. Acad. Sci. U. S. A.* 2020, *117* (18), 9733–9740.
 https://doi.org/10.1073/pnas.1916711117.
- (45) Vansco, M. F.; Caravan, R. L.; Zuraski, K.; Winiberg, F. A. F.; Au, K.; Trongsiriwat, N.; Walsh, P. J.; Osborn, D. L.; Percival, C. J.; Khan, M. A. H.; Shallcross, D. E.; Taatjes, C.

- A.; Lester, M. I. Experimental Evidence of Dioxole Unimolecular Decay Pathway for Isoprene-Derived Criegee Intermediates. *J. Phys. Chem. A* **2020**, *124* (18), 3542–3554. https://doi.org/10.1021/acs.jpca.0c02138.
- (46) Vansco, M. F.; Marchetti, B.; Lester, M. I. Electronic Spectroscopy of Methyl Vinyl Ketone Oxide: A Four-Carbon Unsaturated Criegee Intermediate from Isoprene Ozonolysis. *J. Chem. Phys.* 2018, 149 (24), 244309. https://doi.org/10.1063/1.5064716.
- (47) Vansco, M. F.; Marchetti, B.; Trongsiriwat, N.; Bhagde, T.; Wang, G.; Walsh, P. J.;
 Klippenstein, S. J.; Lester, M. I. Synthesis, Electronic Spectroscopy, and Photochemistry
 of Methacrolein Oxide: A Four-Carbon Unsaturated Criegee Intermediate from Isoprene
 Ozonolysis. J. Am. Chem. Soc. 2019, 141 (38), 15058–15069.
 https://doi.org/10.1021/jacs.9b05193.
- (48) Yin, C.; Takahashi, K. How Big Is the Substituent Dependence of the Solar Photolysis Rate of Criegee Intermediates? *Phys. Chem. Chem. Phys.* **2018**, *20* (23), 16247–16255. https://doi.org/10.1039/C8CP02015A.
- (49) McCoy, J. C.; Marchetti, B.; Thodika, M.; Karsili, T. N. V. A Simple and Efficient Method for Simulating the Electronic Absorption Spectra of Criegee Intermediates: Benchmarking on CH2OO and CH3CHOO. *J. Phys. Chem. A* 2021. https://doi.org/10.1021/acs.jpca.1c01074.
- (50) McGillen, M. R.; Curchod, B. F. E.; Chhantyal-Pun, R.; Beames, J. M.; Watson, N.; Khan, M. A. H.; McMahon, L.; Shallcross, D. E.; Orr-Ewing, A. J. Criegee Intermediate-Alcohol Reactions, A Potential Source of Functionalized Hydroperoxides in the Atmosphere. ACS Earth Sp. Chem. 2017, 1 (10), 664–672. https://doi.org/10.1021/acsearthspacechem.7b00108.

- (51) Yu, X.; Hou, H.; Wang, B. Atmospheric Chemistry of Perfluoro-3-Methyl-2-Butanone [CF3C(O)CF(CF3)2]: Photodissociation and Reaction with OH Radicals. *J. Phys. Chem. A* **2018**, *122* (45), 8840–8848. https://doi.org/10.1021/acs.jpca.8b09111.
- (52) Francés-Monerris, A.; Carmona-García, J.; Acuña, A. U.; Dávalos, J. Z.; Cuevas, C. A.; Kinnison, D. E.; Francisco, J. S.; Saiz-Lopez, A.; Roca-Sanjuán, D. Photodissociation Mechanisms of Major Mercury(II) Species in the Atmospheric Chemical Cycle of Mercury. *Angew. Chemie Int. Ed.* 2020, 59 (19), 7605–7610. https://doi.org/https://doi.org/10.1002/anie.201915656.
- (53) Prlj, A.; Ibele, L. M.; Marsili, E.; Curchod, B. F. E. On the Theoretical Determination of Photolysis Properties for Atmospheric Volatile Organic Compounds. *J. Phys. Chem. Lett.* 2020, 11 (14), 5418–5425. https://doi.org/10.1021/acs.jpclett.0c01439.
- (54) Röder, A.; de Oliveira, N.; Grollau, F.; Mestdagh, J.-M.; Gaveau, M.-A.; Briant, M. Vacuum-Ultraviolet Absorption Spectrum of 3-Methoxyacrylonitrile. *J. Phys. Chem. A* 2020, 124 (45), 9470–9477. https://doi.org/10.1021/acs.jpca.0c08974.
- (55) Rodrigues, G. P.; Ventura, E.; Andrade do Monte, S.; Barbatti, M. UV-Photoexcitation and Ultrafast Dynamics of HCFC-132b (CF2ClCH2Cl). *J. Comput. Chem.* **2016**, *37* (7), 675–683. https://doi.org/https://doi.org/10.1002/jcc.24260.
- (56) Saiz-Lopez, A.; Sitkiewicz, S. P.; Roca-Sanjuán, D.; Oliva-Enrich, J. M.; Dávalos, J. Z.; Notario, R.; Jiskra, M.; Xu, Y.; Wang, F.; Thackray, C. P.; Sunderland, E. M.; Jacob, D. J.; Travnikov, O.; Cuevas, C. A.; Acuña, A. U.; Rivero, D.; Plane, J. M. C.; Kinnison, D. E.; Sonke, J. E. Photoreduction of Gaseous Oxidized Mercury Changes Global Atmospheric Mercury Speciation, Transport and Deposition. *Nat. Commun.* 2018, *9* (1), 4796. https://doi.org/10.1038/s41467-018-07075-3.

- (57) Barbatti, M.; Ruckenbauer, M.; Plasser, F.; Pittner, J.; Granucci, G.; Persico, M.; Lischka, H. Newton-X: A Surface-Hopping Program for Nonadiabatic Molecular Dynamics. *Wiley Interdiscip. Rev. Comput. Mol. Sci.* 2014, 4 (1), 26–33.
 https://doi.org/10.1002/wcms.1158.
- (58) Barbatti, M.; Granucci, G.; Persico, M.; Ruckenbauer, M.; Vazdar, M.; Eckert-Maksić, M.; Lischka, H. The On-the-Fly Surface-Hopping Program System Newton-X: Application to Ab Initio Simulation of the Nonadiabatic Photodynamics of Benchmark Systems. *J. Photochem. Photobiol. A Chem.* 2007, 190 (2), 228–240. https://doi.org/https://doi.org/10.1016/j.jphotochem.2006.12.008.
- (59) Roos, B. O.; Linse, P.; Siegbahn, P. E. M.; Blomberg, M. R. A. A Simple Method for the Evaluation of the Second-Order-Perturbation Energy from External Double-Excitations with a CASSCF Reference Wavefunction. *Chem. Phys.* 1982, 66 (1), 197–207. https://doi.org/https://doi.org/10.1016/0301-0104(82)88019-1.
- (60) Andersson, K.; Malmqvist, P. A.; Roos, B. O.; Sadlej, A. J.; Wolinski, K. Second-Order Perturbation Theory with a CASSCF Reference Function. *J. Phys. Chem.* 1990, 94 (14), 5483–5488. https://doi.org/10.1021/j100377a012.
- (61) Andersson, K.; Malmqvist, P.; Roos, B. O. Second-order Perturbation Theory with a
 Complete Active Space Self-consistent Field Reference Function. *J. Chem. Phys.* 1992, 96
 (2), 1218–1226. https://doi.org/10.1063/1.462209.
- (62) Dunning, T. H. Gaussian Basis Sets for Use in Correlated Molecular Calculations. I. The Atoms Boron through Neon and Hydrogen. *J. Chem. Phys.* 1989, 90 (2), 1007–1023. https://doi.org/10.1063/1.456153.
- (63) Yanai, T.; Tew, D. P.; Handy, N. C. A New Hybrid Exchange-Correlation Functional

- Using the Coulomb-Attenuating Method (CAM-B3LYP). *Chem. Phys. Lett.* **2004**, *393* (1), 51–57. https://doi.org/https://doi.org/10.1016/j.cplett.2004.06.011.
- (64) Hehre, W. J.; Stewart, R. F.; Pople, J. A. Self-Consistent Molecular-Orbital Methods. I.
 Use of Gaussian Expansions of Slater-Type Atomic Orbitals. *J. Chem. Phys.* 1969, 51 (6), 2657–2664. https://doi.org/10.1063/1.1672392.
- (65) Hehre, W. J.; Ditchfield, R.; Stewart, R. F.; Pople, J. A. Self-Consistent Molecular Orbital Methods. IV. Use of Gaussian Expansions of Slater-Type Orbitals. Extension to Second-Row Molecules. *J. Chem. Phys.* 1970, 52 (5), 2769–2773. https://doi.org/10.1063/1.1673374.
- (66) National Center for Atmospheric Research TUV model.
- Werner, H.-J.; Knowles, P. J.; Knizia, G.; Manby, F. R.; Schütz, M.; Celani, P.; Györffy, W.; Kats, D.; Korona, T.; Lindh, R.; Mitrushenkov, A.; Rauhut, G.; Shamasundar, K. R.; Adler, T. B.; Amos, R. D.; Bennie, S.; Bernhardsson, A.; Berning, A.; Cooper, D. L.; Deegan, M. J. O.; Dobbyn, A. J.; Eckert, F.; Goll, E.; Hampel, C.; Hesselmann, A.; Hetzer, G.; Hrenar, T.; Jansen, G.; Köppl, C.; Lee, S. J. R.; Liu, Y.; Lloyd, A. W.; Ma, Q.; Mata, R. A.; May, A. J.; McNicholas, S. J.; Meyer, W.; III, T. F. M.; Mura, M. E.; Nicklass, A.; O'Neill, D. P.; Palmieri, P.; Peng, D.; Pflüger, K.; Pitzer, R.; Reiher, M.; Shiozaki, T.; Stoll, H.; Stone, A. J.; Tarroni, R.; Thorsteinsson, T.; Wang, M.; Welborn, M. MOLPRO, Version 2018.1, a Package of Ab Initio Programs. 2018.
- (68) Werner, H.-J.; Knowles, P. J.; Knizia, G.; Manby, F. R.; Schütz, M. Molpro: A General-Purpose Quantum Chemistry Program Package. *WIREs Comput. Mol. Sci.* **2012**, *2* (2), 242–253. https://doi.org/10.1002/wcms.82.
- (69) , M. J. Frisch, G. W. Trucks, H. B. Schlegel, G. E. Scuseria, M. A. Robb, J. R.

- Cheeseman, G. Scalmani, V. Barone, G. A. Petersson, H. Nakatsuji, X. Li, M. Caricato, A. V. Marenich, J. Bloino, B. G. Janesko, R. Gomperts, B. Mennucci, H. P. Hratchian, J. V, and D. J. F. Gaussian 16, Revision C.01. *Gaussian Inc. Wallingford CT* **2016**.
- (70) Barber, V. P.; Pandit, S.; Green, A. M.; Trongsiriwat, N.; Walsh, P. J.; Klippenstein, S. J.; Lester, M. I. Four-Carbon Criegee Intermediate from Isoprene Ozonolysis: Methyl Vinyl Ketone Oxide Synthesis, Infrared Spectrum, and OH Production. *J. Am. Chem. Soc.* 2018, 140 (34), 10866–10880. https://doi.org/10.1021/jacs.8b06010.
- (71) Caravan, R. L.; Vansco, M. F.; Au, K.; Khan, M. A. H.; Li, Y.-L.; Winiberg, F. A. F.;
 Zuraski, K.; Lin, Y.-H.; Chao, W.; Trongsiriwat, N.; Walsh, P. J.; Osborn, D. L.; Percival,
 C. J.; Lin, J. J.-M.; Shallcross, D. E.; Sheps, L.; Klippenstein, S. J.; Taatjes, C. A.; Lester,
 M. I. Direct Kinetic Measurements and Theoretical Predictions of an Isoprene-Derived
 Criegee Intermediate. *Proc. Natl. Acad. Sci.* 2020, *117* (18), 9733 LP 9740.
 https://doi.org/10.1073/pnas.1916711117.
- (72) Vansco, M. F.; Marchetti, B.; Lester, M. I. Electronic Spectroscopy of Methyl Vinyl Ketone Oxide: A Four-Carbon Unsaturated Criegee Intermediate from Isoprene Ozonolysis. *J. Chem. Phys.* 2018, *149* (24), 244309. https://doi.org/10.1063/1.5064716.
- (73) Lin, Y.-H.; Yang, C.-H.; Takahashi, K.; Lin, J. J.-M. Kinetics of Unimolecular Decay of Methyl Vinyl Ketone Oxide, an Isoprene-Derived Criegee Intermediate, under Atmospherically Relevant Conditions. *J. Phys. Chem. A* 2020, *124* (45), 9375–9381. https://doi.org/10.1021/acs.jpca.0c07928.
- (74) Lin, Y.-H.; Yin, C.; Takahashi, K.; Lin, J. J.-M. Surprisingly Long Lifetime of Methacrolein Oxide, an Isoprene Derived Criegee Intermediate, under Humid Conditions. *Commun. Chem.* 2021, 4 (1), 12. https://doi.org/10.1038/s42004-021-00451-z.

- (75) Vereecken, L.; Novelli, A.; Taraborrelli, D. Unimolecular Decay Strongly Limits the Atmospheric Impact of Criegee Intermediates. *Phys. Chem. Chem. Phys.* **2017**, *19* (47), 31599–31612. https://doi.org/10.1039/C7CP05541B.
- (76) Caravan, R. L.; Vansco, M. F.; Lester, M. I. Open Questions on the Reactivity of Criegee Intermediates. *Commun. Chem.* **2021**, *4* (1), 44. https://doi.org/10.1038/s42004-021-00483-5.
- (77) Khan, M. A. H.; Schlich, B.-L.; Jenkin, M. E.; Cooke, M. C.; Derwent, R. G.; Neu, J. L.; Percival, C. J.; Shallcross, D. E. Changes to Simulated Global Atmospheric Composition Resulting from Recent Revisions to Isoprene Oxidation Chemistry. *Atmos. Environ.* 2021, 244, 117914. https://doi.org/https://doi.org/10.1016/j.atmosenv.2020.117914.
- (78) Crespo-Otero, R.; Barbatti, M. Spectrum Simulation and Decomposition with Nuclear Ensemble: Formal Derivation and Application to Benzene, Furan and 2-Phenylfuran. *Theor. Chem. Acc.* **2012**, *131* (6), 1–14. https://doi.org/10.1007/s00214-012-1237-4.
- (79) Crespo-Otero, R.; Barbatti, M. Recent Advances and Perspectives on Nonadiabatic Mixed Quantum–Classical Dynamics. *Chem. Rev.* 2018, 118 (15), 7026–7068. https://doi.org/10.1021/acs.chemrev.7b00577.
- (80) Sršeň, Š.; Sita, J.; Slavíček, P.; Ladányi, V.; Heger, D. Limits of the Nuclear Ensemble Method for Electronic Spectra Simulations: Temperature Dependence of the (E)-Azobenzene Spectrum. *J. Chem. Theory Comput.* 2020, 16 (10), 6428–6438. https://doi.org/10.1021/acs.jctc.0c00579.
- (81) Xue, B.-X.; Barbatti, M.; Dral, P. O. Machine Learning for Absorption Cross Sections. *J. Phys. Chem. A* **2020**, *124* (35), 7199–7210. https://doi.org/10.1021/acs.jpca.0c05310.

For Table of Contents Only

